

SRI International

AD-A273 031



Quarterly Technical Report 5 • 11 November 1993

IR MATERIALS PRODUCIBILITY

M.A. Berding, Sr. Research Physicist
Physical Electronics Laboratory

SRI Project 3820

Prepared for:

Contracting Officer's Technical Representative
Advanced Research Projects Agency
Microelectronics Technology Office (MTO)
3701 N. Fairfax Drive
Arlington, VA 22203-1714

Attn: Mr. Raymond Balcerak

ARPA Order No. 8557; Program Code Nos. 2H20, 2D10

Contract MDA972-92-C-0053

Covering the period: 1 August through 31 October 1993

The views and conclusions contained in this document are those of the authors and should not be interpreted as representing the official policies, either expressed or implied, of the Advanced Research Projects Agency or the U.S. Government.

APPROVED FOR PUBLIC RELEASE
DISTRIBUTION UNLIMITED

S DTIC
ELECTE
NOV 26 1993
A

93-28897



93 11 24 050

IR MATERIALS PRODUCIBILITY

M.A. Berding, Sr. Research Physicist
Physical Electronics Laboratory

SRI Project 3820

Prepared for:

Contracting Officer's Technical Representative
Advanced Research Projects Agency
Microelectronics Technology Office (MTO)
3701 N. Fairfax Drive
Arlington, VA 22203-1714

Attn: Mr. Raymond Balcerak

ARPA Order No. 8557; Program Code Nos. 2H20, 2D10

Contract MDA972-92-C-0053

Covering the period: 1 August through 31 October 1993

The views and conclusions contained in this document are those of the authors and should not be interpreted as representing the official policies, either expressed or implied, of the Advanced Research Projects Agency or the U.S. Government.

APPROVED FOR PUBLIC RELEASE
DISTRIBUTION UNLIMITED

Accession For	
NTIS CRA&I	<input checked="" type="checkbox"/>
DTIC TAB	<input type="checkbox"/>
Unannounced	<input type="checkbox"/>
Justification	
By	
Distribution/	
Availability Codes	
Dist	Avail and/or Special
A-1	

Approved:

Eric Pearson, Director
Physical Electronics Laboratory

Donald L. Nielson, Vice President
Computing and Engineering Sciences Division

REPORT DOCUMENTATION PAGE

Form Approved
OMB No. 0704-0188

Public reporting burden for this collection of information is estimated to average 1 hour per response, including the time for reviewing instructions, searching existing data sources, gathering and maintaining the data needed, and completing and reviewing the collection of information. Send comments regarding this burden estimate or any other aspect of this collection of information, including suggestions for reducing this burden, to Washington Headquarters Services, Directorate for Information Operations and Reports, 1215 Jefferson Davis Highway, Suite 1204, Arlington, VA 22202-4302, and to the Office of Management and Budget, Paperwork Reduction Project (0704-0188), Washington, DC 20503.

1. AGENCY USE ONLY (Leave Blank)	2. REPORT DATE <p style="text-align: center;">11 November 1993</p>	3. REPORT TYPE AND DATES COVERED <p style="text-align: center;">Quarterly Tech. Rpt. 5, 8-1-93 to 10-31-93</p>	
4. TITLE AND SUBTITLE <p>IR Materials Producibility</p>		5. FUNDING NUMBERS	
6. AUTHORS <p>M.A. Berding, SRI International</p>		8. PERFORMING ORGANIZATION REPORT NUMBER	
7. PERFORMING ORGANIZATION NAME(S) AND ADDRESS(ES) <p style="text-align: center;">SRI International 333 Ravenswood Avenue Menlo Park, CA 94025-3493</p>		10. SPONSORING/MONITORING AGENCY REPORT NUMBER	
9. SPONSORING/MONITORING AGENCY NAME(S) AND ADDRESS(ES) <p>Advanced Research Projects Agency Microelectronics Technology Office (MTO), Infrared Focal Plane Array Program 3701 N. Fairfax Drive Arlington, VA 22203-1714</p>		11. SUPPLEMENTARY NOTES	
12a. DISTRIBUTION/AVAILABILITY STATEMENT <p>Approved for public release; distribution unlimited</p>		12b. DISTRIBUTION CODE	
<p>13. ABSTRACT (<i>Maximum 200 words</i>)</p> <p>This quarter we have focused on completing a paper containing the details of our calculations on the defect concentration in $x = 0.2 \text{ Hg}_{1-x}\text{Cd}_x\text{Te}$. This has involved the refinement of the calculations of all the defects. We have continued to develop our ideas about the formation and annihilation of tellurium precipitates in HgCdTe. We have presented our work on dislocations and the reanalysis of the electronic band structure of narrow-gap HgCdTe at the IRIS materials meeting in August and at the MCT Workshop in October. A paper on the electronic mobility in $\text{Hg}_{0.78}\text{Cd}_{0.22}\text{Te}$ has been submitted for publication in the <i>Journal of Applied Physics</i>.</p> <p>We have completed the calculations of the lithium vacancy and niobium antisite formation energies in LiNbO_3, and have begun to incorporate these energies into a thermodynamical analysis. We have continued to refine our calculations on the defect concentrations in ZnSe and have made preliminary predictions of the dominant defects in that system.</p>			
14. SUBJECT TERMS <p>native point defect; defect density; photonic material; IRFPA; HgTe; CdTe; ZnSe; HgCdTe; LiNbO_3; dislocation; Boltzmann transport equation</p>		15. NUMBER OF PAGES <p style="text-align: center;">24</p>	
16. PRICE CODE		17. SECURITY CLASSIFICATION OF REPORT <p style="text-align: center;">Unclassified</p>	
18. SECURITY CLASSIFICATION OF THIS PAGE <p style="text-align: center;">Unclassified</p>		19. SECURITY CLASSIFICATION OF ABSTRACT <p style="text-align: center;">Unclassified</p>	
20. LIMITATION OF ABSTRACT <p style="text-align: center;">Unlimited</p>			

SUMMARY

The work summarized in this report covers the fifth quarter of a program with a goal that is twofold: first, to study the properties of native point defect in infrared focal-plan array (IRFPA) active and substrate materials, and second, to study the properties of native point defects in two classes of photonic materials, the wide-gap II-VI compounds (ZnSe as the prototype for which impurity properties will also be calculated) and the nonlinear optical materials (LiNbO₃ as the prototype). Our accomplishments in the fifth quarter include

- Refinement of our calculations of the native defect formation energies in HgCdTe
- Writing a comprehensive paper on the results of our work on the defect concentration in HgCdTe and their impact on device performance
- Beginning the calculations of the native defect formation energies in CdTe
- Refinement of our calculations of the native defect formation energies in ZnSe
- Preliminary thermodynamical analysis of the defect concentrations in ZnSe
- Calculation of two defect formation energies in LiNbO₃: the lithium vacancy and the niobium antisite
- Completion of a paper on the electron mobility in Hg_{0.22}Cd_{0.78}Te from a solution of the full Boltzmann transport equation with Fermi-Dirac statistics and an accurate band structure
- Presentation of four papers at technical meetings on the results of our work on dislocations and the band structure and transport properties of HgCdTe

CONTENTS

1	DEFECTS IN MCT, HgTe, CdTe, and ZnTe	1
2	DISLOCATIONS IN MCT	1
3	TRANSPORT PROPERTIES OF HgCdTe	1
4	WIDE-GAP II-VI COMPOUNDS (ZnSe AS PROTOTYPE)	1
5	NONLINEAR OPTICAL MATERIALS (LiNbO ₃ AS THE PROTOTYPE)	2
6	WORK PLANNED	3
	APPENDIX: ELECTRON MOBILITY IN Hg _{0.8} Cd _{0.2} Te ALLOY	A-1

1. DEFECTS IN MCT, HgTe, CdTe, and ZnTe

During this quarter we have worked on refining our calculations of the defect formation energies in HgTe that are used to predict the defect concentrations in $\text{Hg}_{0.8}\text{Cd}_{0.2}\text{Te}$. This has involved completion of self-consistent calculations for all the defects and calculations of the gradient correction energies within the full-potential codes. In addition some small numerical problems were resolved. Once we have finished these calculations, we will complete our long paper on defects in $\text{Hg}_{0.8}\text{Cd}_{0.2}\text{Te}$.

We have begun to consider the mercury vacancy—tellurium antisite pair. We expect that this defect complex may be important because both its constituents are present in relatively high densities, and because they should be attracted to one another by both Coulomb and strain field. We have set up to do the calculations, and are just waiting for the computational resources to become available to complete the calculations.

The calculations of the defect formation energies in CdTe have begun. Once again, we are waiting for computational resources to be freed up to continue these calculations.

2. DISLOCATIONS IN MCT

Our work on dislocations in HgCdTe and their impact on device performance was presented at the 1993 Materials IRIS Meeting in August 1993 and at the 1993 U.S. Workshop on the Physics and Chemistry of Mercury Cadmium Telluride and Other IR Materials. Copies of these papers have been forwarded to ARPA under separate cover.

3. TRANSPORT PROPERTIES OF HgCdTe

We have completed a paper on the reanalysis of the electron mobility in $\text{Hg}_{0.78}\text{Cd}_{0.22}\text{Te}$. The electron mobility was calculated by solving the Boltzmann transport equation with Fermi-Dirac statistics and a full band structure. The calculated values are in excellent agreement with experiments, and effects of various traditional approximations are discussed. The Appendix is a preprint of this paper.

4. WIDE-GAP II-VI COMPOUNDS (ZnSe AS PROTOTYPE)

We have continued our calculation of the point defect energies in ZnSe. In our third quarterly report, we discussed preliminary results. During this quarter, we have refined and extended these calculations. First, we have found that a larger basis set size was necessary to achieve the accuracy required for these calculations (less than 0.1 eV). Thus, the calculations for the eight defects (the zinc and selenium vacancy, the zinc and selenium antisites, and the zinc and selenium atoms at two different tetrahedral interstitial sites) have been extended to larger basis set sizes this quarter. In addition, we have begun the calculation of the gradient corrections for all the defects. Previously, we had estimated these energies based on the atomic spheres

approximation version of the linearized muffin-tin orbital (LMTO) method, but have extended these calculations using the more accurate full potential, again because of the accuracy in the energies that is required to predict the defect densities reliably.

5. NONLINEAR OPTICAL MATERIALS (LiNbO₃ AS THE PROTOTYPE)

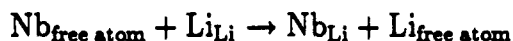
As discussed in the previous report, we are studying the defect structure of LiNbO₃ using a reliable first-principles electronic structure method, the LMTO. We are using the same techniques for calculating the defect energies as we have applied to the defects in HgCdTe and ZnSe, and as reported in some detail in earlier reports.

Several models have been proposed of the defect structure in LiNbO₃ relating to the excess niobium in the lattice. To date, these models are based exclusively on experimental information. The first model that we are addressing involves a niobium antisite (Nb_{Li}) that has a 4+ valency, that is charge compensated by four lithium vacancies (V_{Li}) that each have a 1- valency. The second model that we are examining involves an arrangement of cations along the polar axis out of normal sequence such that two niobium antisites are separated by a niobium vacancy, so as to cancel the dipole. In addition to these, other models have been proposed, each of which explains a specific experiment, but an overall defect picture is still lacking. Because of the sensitive dependence of various defects on growth conditions, various characterization techniques and possibly small activation energy difference more than one defect structure may have been seen.

In this quarter, we calculated the activation energies of the two most likely defects the lithium vacancy V_{Li} and niobium antisite, Nb_{Li}. The problem is approached using a supercell model with a full-potential LMTO electronic structure method. There is a computational limit to the number of defects that can be included. We start with a 30-atom unit cell with one defect.

In the case of V_{Li} vacancy, after removing a lithium atom, the structure is relaxed to minimize its total energy. We find that the three oxygen atoms in the plane of removed lithium and the niobium atoms on the c-axis move toward the vacancy. The relaxation is relatively small with a displacement of about 0.03 Å and an energy gain of about 125 meV. We find that the vacancy formation energy is 5.10 eV (endothermic).

Historically, it is believed that Nb_{Li} is favored. We have carried out the first quantitatively accurate calculation of the formation energy. Unlike V_{Li}, Nb_{Li} relaxes considerably by 0.2 Å. Although the oxygen atoms on the lithium plane move very little, the other set of oxygen atoms that form an octahedron about the Nb_{Li} move as much as 0.3 Å. In addition, all niobium atoms and the nearest lithium atoms move with a maximum displacement of about 0.03 Å. Mostly, the relaxation is radially away from the defect. Because of large lattice relaxation about the niobium antisite, there is a large relaxation energy of 1.2 eV. It is interesting that the reaction to form a niobium antisite by exchanging a niobium in the free atom state with a lithium in the free atom state via the reaction



is exothermic with an energy of -11.6 eV. This implies that niobium antisite will probably be an important defect in LiNbO_3 . Of course, one needs to include the long-range Coulomb energies associated the Nb_{Li} , and the energies associated with the exchange of a niobium with a lithium in the vapor phase to complete the calculation.

From these two defect calculations, we can make some preliminary comments on the model that proposed that one Nb_{Li} is associated with four V_{Li} . The direct gap LiNbO_3 is 3.5 eV. If we assume that the acceptor-like state created by the lithium vacancy is near the top of the valance band and the donor-like Nb_{Li} state is near the bottom of the conduction band, there will be a gain of 3.5 eV due to charge transfer. Noting that V_{Li} and Nb_{Li} formation energies are 5.1 eV and -11.6 eV, respectively, we get a formation energy of -5.2 eV for Nb antisite with four Li vacancies. Refinements in the calculation will be necessary to complete this analysis - for example, inclusion of the gradient corrections.

These calculations address the defect formation energies only, and were done within the local density approximation. To make quantitative predictions of the defect concentrations, one must include a number of additional factors. First, we must add to the local density energies a gradient correction, which generally brings our results into better agreement with experiments. We have discussed this gradient correction at some length in our previous quarterly reports. In addition, we must make some quantitative predictions of the localized states associated with the various defects. We must also add a contribution to the defect formation free energy from the change in the vibrational spectrum of the solid upon formation of a defect. We have calculated this free energy contribution in HgTe and ZnSe using a valence force field model for the zincblende lattice. We must extend these calculations to the LiNbO_3 lattice. Finally, we must complete the thermodynamic defect density calculation including the free energy of the species in the vapor phase. We have completed such calculations for HgCdTe and found remarkable agreement with experiment, given that (with the exception of the temperature dependence of the band-gap energy) the calculations were *ab initio*. We are extending our codes to examine the LiNbO_3 .

6. WORK PLANNED

We will be finishing our work on the gradient corrections and writing a paper on the results; this paper will be essential to the support of our work on the defects in HgCdTe, ZnSe, and LiNbO_3 . This paper was not completed in this quarter because one of our group members who was doing some of the calculations was on sabbatical leave in Japan for the summer. We expect to complete our paper on defects in HgCdTe for submission to *Physical Review B*. This paper was not completed this quarter, in large part because of the lack of adequate computational resources. We will continue our study of defects in CdTe this next quarter and begin the calculation of the defect energy of the mercury vacancy—tellurium antisite pair. A preliminary analysis of the defect concentrations as a function of temperature and pressure in ZnSe will be completed. We will complete the gradient correction energies of LiNbO_3 and make preliminary predictions of the dominant defects in the system.

APPENDIX
ELECTRON MOBILITY IN $\text{Hg}_{0.78}\text{Cd}_{0.22}\text{Te}$ ALLOY

ELECTRON MOBILITY IN $\text{Hg}_{0.78}\text{Cd}_{0.22}\text{Te}$ ALLOY

Srinivasan Krishnamurthy and Arden Sher

SRI International, Menlo Park, CA 94025

ABSTRACT

The electron mobility in $\text{Hg}_{0.78}\text{Cd}_{0.22}\text{Te}$ is calculated by solving the Boltzmann transport equation with Fermi-Dirac statistics and a full band structure. The calculated values are in excellent agreement with experiments, and effects of various traditional approximations are discussed.

PACS numbers: 72.20.Fr, 72.10.-d, 72.28.+d, 72.20.-i

The experimental results on electron transport properties of semiconductors are often compared to theory that rests on three approximations, namely, parabolic band structures for those states occupied in the measurement, Maxwell-Boltzmann (MB) statistics, and the collision time approximation to full Boltzmann gain-loss equation solutions. These approximations are made to all scattering mechanisms whether they are elastic or inelastic. It is well known that, even in large-gap materials, the constant effective mass approximation is valid only very near (within $\sim E_g/10$) to the band edge.^{1,2} This approximation has been recognized to be particularly poor for narrow-gap materials, and nonparabolic corrections calculated in the $\mathbf{k}\cdot\mathbf{p}$ formalism are often used.^{3,4,5} This correction is substantial but still differs considerably from our more accurately calculated band structures. In addition, our fit of the conduction band to an analytical function makes many results transparent and simplifies the calculations. As the Fermi energy can easily move into the conduction band of lightly doped narrow-gap materials, the form of the Boltzmann equation with Fermi-Dirac (FD)—instead of the usual MB—statistics must be used to obtain accurate transport coefficients.

In the literature, an iterative solution to the Boltzmann transport equation (BTE) with FD statistics has been derived.⁶ Although this method can yield nearly exact solutions by including more terms in the expansion and with more iterations, it can be time-consuming since the procedure has to be repeated for every crystal wave vector \mathbf{k} . In this paper, we derive an alternate method that first simplifies BTE with FD statistics to the point where the solution for full band structures can be obtained by successive substitution. This method is applied to the study of electron mobility as a function of temperature T and impurity concentration n_D in a $\text{Hg}_{0.78}\text{Cd}_{0.22}\text{Te}$ alloy. Results are compared with experiments.

We start from the BTE of a homogeneous medium obeying FD statistics. We have

$$\frac{df(\mathbf{k})}{dt} = \sum_{\mathbf{k}'} \left[w(\mathbf{k}, \mathbf{k}') f(\mathbf{k}') (1 - f(\mathbf{k})) - w(\mathbf{k}', \mathbf{k}) f(\mathbf{k}) (1 - f(\mathbf{k}')) \right] \quad (1)$$

The first term of the right side of Eq. (1) is the gain term, and the second one is the loss term. In equilibrium, the left side is identically zero and because, in general for a system of interest interacting with a heat bath,⁷ $w(\mathbf{k}, \mathbf{k}') e^{-\beta E_{\mathbf{k}'}} = w(\mathbf{k}', \mathbf{k}) e^{-\beta E_{\mathbf{k}}}$, f becomes the equilibrium FD distribution function f_0 given by

$$f_0(E_{\mathbf{k}}) = (e^{\beta(E_{\mathbf{k}} - \epsilon_F)} + 1)^{-1} \quad (2)$$

where β is $(k_B T)^{-1}$. In the presence of an electric field,

$$\frac{df(\mathbf{k})}{dt} = \frac{\partial f(\mathbf{k})}{\partial t} + \nabla f(\mathbf{k}) \cdot \frac{\mathbf{e}E}{\hbar} \quad (3)$$

In steady state, the $\partial f(\mathbf{k})/\partial t$ in Eq. (3) vanishes. The solution $f(\mathbf{k})$ can always be written as a sum of $f_0(\mathbf{k})$ and some deviation $\Delta(\mathbf{k})$. That is,

$$f(\mathbf{k}) = f_0(\mathbf{k}) + \Delta(\mathbf{k}) \quad (4)$$

Note that $\sum_{\mathbf{k}} \Delta(\mathbf{k})$ is zero for a sample with ohmic contacts because the number of electrons should remain constant. Combining Eq. (1) through Eq. (4), we get

$$\begin{aligned} \nabla f(\mathbf{k}) \cdot \frac{\mathbf{e}E}{\hbar} = \sum_{\mathbf{k}'} [W(\mathbf{k}, \mathbf{k}') \Delta(\mathbf{k}') - W(\mathbf{k}', \mathbf{k}) \Delta(\mathbf{k}) \\ + (w(\mathbf{k}', \mathbf{k}) - w(\mathbf{k}, \mathbf{k}')) \Delta(\mathbf{k}) \Delta(\mathbf{k}')] \end{aligned} \quad (5)$$

where the renormalized W and the usual transition probability per unit time w are related by

$$W(\mathbf{k}, \mathbf{k}') = w(\mathbf{k}, \mathbf{k}') \frac{(1 - f_0(\mathbf{k}))}{(1 - f_0(\mathbf{k}'))} \quad (6)$$

Note that for elastic scattering W and w are equal. However, for inelastic cases the relative size of W to w depends on whether energies at \mathbf{k} and \mathbf{k}' are larger or smaller than ϵ_F . If both initial and final energies are larger (or smaller) than ϵ_F , then only small corrections to w occur. However, if the initial state is above ϵ_F and the final state is below ϵ_F , then for that scattering event W is suppressed. This tends, for example, to decrease the contribution of inelastic scattering events involving phonon emission. Also notice that if the perturbation is

small, then the Δ^2 term can be neglected and Eq. (5) resembles the traditional MB steady-state BTE where W plays the role of w .

We further expand $\Delta(\mathbf{k})$ in power series of an indexing parameter λ , which we will eventually set to unity. Thus,

$$\Delta(\mathbf{k}) = \sum_{n=1}^{\infty} f_n(\mathbf{k}) \lambda^n \quad (7)$$

Substituting Eq. (7) in Eq. (5) and noting that $f(\mathbf{k})$ has one additional term, we get,

$$\begin{aligned} \sum_{n=0}^{\infty} \nabla f_n(\mathbf{k}) \cdot \frac{\mathbf{e}}{\hbar} E \lambda^{n+1} &= \sum_{\mathbf{k}', n=1}^{\infty} [W(\mathbf{k}, \mathbf{k}') f_n(\mathbf{k}') - W(\mathbf{k}', \mathbf{k}) f_n(\mathbf{k})] \lambda^n \\ &+ \sum_{\mathbf{k}', n, n'=1}^{\infty} [w(\mathbf{k}', \mathbf{k}) - w(\mathbf{k}, \mathbf{k}')] f_n(\mathbf{k}) f_{n'}(\mathbf{k}') \lambda^{n+n'} \end{aligned} \quad (8)$$

By equating the coefficients of the same power of λ on both sides, we get a series of equations:

$$\nabla f_0(\mathbf{k}) \cdot \frac{\mathbf{e}}{\hbar} E = \sum_{\mathbf{k}'} [W(\mathbf{k}, \mathbf{k}') f_1(\mathbf{k}') - W(\mathbf{k}', \mathbf{k}) f_1(\mathbf{k})] \quad (9a)$$

$$\begin{aligned} \nabla f_0(\mathbf{k}) \cdot \frac{\mathbf{e}}{\hbar} E &= \sum_{\mathbf{k}'} [W(\mathbf{k}, \mathbf{k}') f_2(\mathbf{k}') - W(\mathbf{k}', \mathbf{k}) f_2(\mathbf{k}) \\ &+ (w(\mathbf{k}', \mathbf{k}) - w(\mathbf{k}, \mathbf{k}')) f_1(\mathbf{k}) f_1(\mathbf{k}')] \end{aligned} \quad (9b)$$

and so on

Knowing f_0 (from Eq. (2)), Eq. (9a) is solved for f_1 and the solution is used (Eq. (9b)) for f_2 and so on. This procedure can be continued to the required precision. We emphasize that for low electric fields, only the lowest-order equation (9a) needs to be solved to obtain accurate answers. When hot electron effects are addressed, iterative solutions should be used.

This procedure reduces the original integro-differential equation (5) to that of solving the following integral equation.

$$C(\mathbf{k}) = \sum_{\mathbf{k}'} [W(\mathbf{k}, \mathbf{k}') g(\mathbf{k}') - W(\mathbf{k}', \mathbf{k}) g(\mathbf{k})] \quad (10)$$

where $C(\mathbf{k})$ is a known function and $g(\mathbf{k})$ can be any of the set $\{f_n\}$. One of the fastest ways to solve for $g(\mathbf{k})$ is by expanding it in terms of an orthonormal basis set $\{\Phi(\mathbf{k})\}$. That is, take

$$g(\mathbf{k}) = \sum_n a_n \Phi_n(\mathbf{k}) \quad (11)$$

Substituting Eq. (11) in Eq. (10), multiplying both sides by $\Phi_m(\mathbf{k})$ and then summing over \mathbf{k} yields a matrix equation $C = AW$, where A is a row matrix of the required expansion coefficients. We see that A can be easily obtained by multiplying the square matrix W^{-1} by the row matrix C . The size of the matrix W is determined by the number of functions in the basis set. If the basis set is complete, the solution is exact. However, if the perturbation is small, one can truncate the basis set and obtain accurate solutions with only a few functions. For applied electric fields up to 7 kV/cm, eight basis functions were shown to be sufficient.^{8,9} Hence, in principle, following this procedure all f_n and the final distribution function can be obtained.

The formalism developed above to find solutions to BTE with FD statistics can be used to calculate the mobility μ from the following expression,

$$\mu = \frac{e}{\hbar} \frac{\sum_{n,\mathbf{k}} a_n v(\mathbf{k}) \Phi_n(\mathbf{k})}{\sum_{\mathbf{k}} f_0(\mathbf{k})} \quad (12)$$

where $v(\mathbf{k})$ is the group velocity of an electron in the state \mathbf{k} .

We apply this method to a study of the electron mobility in a $\text{Hg}_{0.78}\text{Cd}_{0.22}\text{Te}$ alloy with 0.1 eV (at 77 K) band gap. We use a high-quality band structure in the calculation. Quantitatively accurate band structures of group IV elements,¹⁰ III-V compounds,¹¹ and II-VI compounds^{11,12} can be obtained using a minimum set of sp^3 orbitals in semiempirical calculations. First, empirical pseudopotential form factors are used to calculate a tight-binding Hamiltonian, H in the minimum set, but with interactions between atoms retained to all ranges. H is then transformed into a zeroth order H_0 in an orthonormal basis. Then a perturbative

Hamiltonian having a first-neighbor tight-binding form is added to H_0 to fine tune the band structure. Because long-range interactions are included in this Hamiltonian, the measured band curvatures as well as symmetry point energies are correctly reproduced. This procedure is followed for both HgTe and CdTe, and then the alloy band structures are calculated in the coherent potential approximation.

We find that the lower part of the calculated conduction band needed for the transport calculations is replicated very well by a hyperbola,

$$E_k = (\gamma k^2 + c^2)^{1/2} - c \quad (13)$$

where γ and c are adjusted to fit the calculated band structure in the energy range of interest.

When γ and c are treated as constants related to the band gap E_g and the effective mass, this expression reduces to the same nonparabolic correction form obtained in the $\mathbf{k}\cdot\mathbf{p}$ method.⁴

However, the numerical values of γ and c are not the same as ours. For example, in the chosen case, γ and c are 48.3 and 0.058, respectively, whereas the corresponding $\mathbf{k}\cdot\mathbf{p}$ values are 36.0 and 0.05. The differences are found to be large enough to cause a noticeable change in the band structure and transport coefficients. The band structure calculated by diagonalizing the Hamiltonian is shown in Fig. 1 (heavy line). We can see that the fitted conduction band structure (thin line) agrees quite well up to an energy level of 0.5 eV from the conduction band edge. In the studies presented here, Eq. (13) can be used as the energy dispersion relation without loss of accuracy, in the transport expressions that follow. Also shown in Fig. 1 is the poor reproduction of the conduction band obtained with parabolic approximation (heavy dashed line) and the usual nonparabolic correction (thin dashed line).

Two qualitative features of the band structure in Fig. 1 that impact transport properties should be noted. First, for energies $E-E_c$ greater than 50 meV where the shape of the conduction band is nearly linear in \mathbf{k} , the group velocity is a constant independent of the \mathbf{k} . Then, the density of states (DOS) increases proportional to E rather than $E^{1/2}$ as in the case of parabolic

bands. Clearly, these features modify the transport properties of electrons occupying these states. The first feature, constant group velocity, eliminates increases in drift velocity arising from increases in electron temperatures. The second feature increases the scattering rates because the density of final states, into which the scattering can occur, is higher than that in a parabolic band. This effect decreases the drift velocity and mobility.

The calculation of the Fermi level ϵ_F as a function temperature T and doping concentration n_D is required for all transport calculations. A knowledge of temperature-dependent gap $E_g(T)$ is essential to obtain ϵ_F . Ideally, temperature dependence should be included by adding the electron phonon interaction to the Hamiltonian from which the variation of E_g with T is obtained. We have developed a general method to incorporate phonon and alloy effects into the same CPA formalism,¹³ but such an approach is not attempted here. Instead, we use an empirical expression first deduced by Hansen, Schmidt and Casstleman¹⁴ given by,

$$E_g = 0.0954 + 0.327T/1000 \quad (14)$$

After studying the effects of various approximations and obtaining trends, the calculations will be repeated with a proper temperature-dependent formalism.

Then ϵ_F is calculated from the condition¹⁵ that at a given T the number of electrons in the conduction band is the sum of electrons excited from the valence band and donor levels. The donor states are assumed to be located at the bottom of the conduction band. The valence and conduction band DOS are calculated from our band structures. The valence band DOS yields a hole effective mass of 0.65. The ϵ_F (measured from the valence band edge) as a function of T and n_D , calculated from the hyperbolic band structures, is given in Fig. 2. The dashed line is the empirical band gap given by Eq. (2).

In the calculation of mobility we include the scattering due to ionized impurities and polar optic phonons whose scattering potentials are, respectively,

$$V_{\text{imp}} = \frac{e^2}{\epsilon_0 r} e^{-\lambda r}$$

$$V_{\text{ep}} = 4\pi i \left(\frac{e^2 \hbar}{2\xi_l \omega_l V} \right)^{1/2} \sum_{\mathbf{q}} a_{\mathbf{q}}^* e^{-i\mathbf{q}\cdot\mathbf{r}} - a_{\mathbf{q}} e^{i\mathbf{q}\cdot\mathbf{r}}$$

with

$$\lambda = \left(\frac{4\pi n_e e^2}{\epsilon k_B T} \right)^{1/2}$$

$$\xi_l^{-1} = \frac{\omega_l^2}{4\pi} (\epsilon_{\infty}^{-1} - \epsilon_0^{-1})$$

where ϵ_0 , ϵ_{∞} are zero and infinite frequency dielectric constants, $\hbar\omega_l$ is the longitudinal optical phonon energy, \mathbf{q} is the phonon wave vector, and $a_{\mathbf{q}}$ is the phonon annihilation operator. n_e is the number of electrons in the conduction band, which is, in general, larger than the number of ionized impurities. Note that the coupling constants are determined from fundamental properties of the material and we have no adjustable parameters to fit the transport data. Hermite polynomials have proved to be a good basis set for solving BTE with FD statistics. However, we find that only the first two basis functions are needed to obtain converged results. Hence, our basis set is $e^{\beta E \mathbf{k}}$ and $\mathbf{k}\cdot\mathbf{E} e^{\beta E \mathbf{k}}$. The resulting mobility is plotted in Fig. 3 (heavy solid line).

Calculated mobilities for various impurity concentrations and temperature are shown in Fig. 3. A peak in the mobility exists for a low concentration of $5 \times 10^{14} \text{ cm}^{-3}$, in agreement with experiment.¹⁶ At low carrier concentration, the Fermi energy lies well into the gap, and consequently only a few impurities are ionized. As the temperature is increased the number of electrons in the conduction band increases, and screening becomes more effective. The increase in the number of ionized impurities is overwhelmed by the increase in screening, and the impurity-limited mobility increases with T . However, once the phonon scattering becomes stronger, the mobility decreases. This competition between impurity and phonon scattering gives rise to a peak in the mobility around 30 K. However, at still lower doping concentration, the impurity scattering is not effective at all, and the mobility then limited only by phonons will continue to increase as T is lowered. At higher doping densities the impurity-limited mobility

also decreases with T because of a large increase in ionized impurities that now dominates the improved screening until very low temperatures are reached, and the peak vanishes. At intermediate doping densities a remnant of the peak is seen. At very high densities and very low temperatures, the screening once again wins, and along with the effects from the Fermi statistics the mobility increases slightly with n_D . This effect may be hard to verify experimentally as the compensation will tend to mask it.

In Fig. 4, we compare the mobilities calculated in various approximations to experiments. The carrier concentration in the calculations was set equal to that in experiments. Two experimental data sets taken on liquid phase epitaxy material^{16,17} are shown in Fig. 4 (dashed lines). The latest set exhibits higher mobilities for the same Hg content and carrier concentration and is presumably a better material. Also shown are the mobilities obtained from the hyperbolic band structure (heavy solid line) and from the $k \cdot p$ band structure (thin solid line). For comparison, mobility obtained in the collision time approximation (dotted line) is also shown.

It is instructional to compare various curves in Fig. 4. All curves are calculated with the same scattering parameters. First our calculated mobilities are higher than those from the $k \cdot p$ band structure. Smaller γ used in the $k \cdot p$ scheme means that DOS is larger, resulting in lower mobility. However, both curves predict a hump in the temperature variation of mobility near 40 K where phonon scattering takes over from impurity scattering, which dominates at lower temperatures. The full solution to BTE in conjunction with the change in the Debye screening length and phonon scattering give rise to this hump. Second, the collision time approximation does not produce this hump. We note that the mobility calculated with a collision time approximation grossly overestimates the scattering rate and wipes out the peak in mobility. A smaller peak near 200 K is due to a change in the Fermi energy.

Our predictions fall within $\pm 25\%$ of the latest experimental values over a temperature range of 10 to 300 K. Calculated values are smaller at low T and larger at high T than in experiment. As the curves in Fig. 3 clearly demonstrate that the electron mobility is a sensitive

function in the shape of the band structure, we must await our better temperature-dependent band structures before improvements are forthcoming. We have already shown from our preliminary studies of absorption coefficient that empirical gaps are as much as 20% too large.¹⁸ If detailed calculations verify these results, then impurity-dominated mobilities will increase at low T, and the neglected scattering mechanisms such as alloy disorder, transverse optical phonons, and acoustic phonons will decrease the mobility at high T to bring the predictions in better agreement with experiment.

In conclusion, we described another method to solve the Boltzmann transport equation with a full band structure and Fermi-Dirac statistics. This method is particularly useful when treating the transport properties of narrow-gap materials where the band structures are nonparabolic and Fermi statistics are essential. The method is applied to the study of electron mobility in a 100-meV band gap (at 77 K) $\text{Hg}_{0.78}\text{Cd}_{0.22}\text{Te}$ alloy. The calculated mobility compares well with the experimental mobility over a wide range of temperatures. Calculated values are 20% smaller at low T and 25% larger at high T than experiment. It appears that the calculated values will be smaller than experimental values at temperatures lower than 10 K. Most important, the observed hump in the mobility (with T) at low carrier concentration and the shape change at higher carrier concentration can be explained without resorting to additional scattering mechanisms or parameters. Further improvements await a proper calculation of the band structure and inclusion of alloy, transverse, and acoustic phonon scattering.

We thank M.A. Berding and A.-B. Chen for many valuable discussions and Dr. J. Bajaj for providing us with experimental mobility data. The work was supported in part by ARPA Contract MDA972-92-C-0053 and ONR Contract N00014-93-C-0091.

REFERENCES

- ¹E.O. Kane, *J. Phys. Chem. Solids* **1**, 249 (1957).
- ²S. Krishnamurthy, A. Sher, and A.-B. Chen, *J. Appl. Phys.* **61**, 1475 (1987).
- ³J.L. Schmidt, *J. Appl. Phys.* **41**, 2876 (1970).
- ⁴J.R. Meyer and F.J. Bartoli, *J. Vac. Sci. Technol.* **21**, 237 (1982).
- ⁵F.J. Bartoli, J.R. Meyer, R.E. Allen, and C.A. Hoffman, *J. Vac. Sci. Technol.* **21**, 241 (1982).
- ⁶D.L. Rode, *Semiconductors and Semimetals* **10**, 15 (1972).
- ⁷A. Sher, and H. Primikoff, *Phys. Rev. B* **119**, 178 (1964).
- ⁸S. Krishnamurthy, S., A. Sher, and A.-B. Chen, 1989: *Appl. Phys. Lett.* **55**, 1003.
- ⁹S. Krishnamurthy and M. van Schilfgaarde, *Computational Electronics* (Klewer, Boston), p. 119 (1990).
- ¹⁰S. Krishnamurthy, A. Sher, and A.-B. Chen, *Phys. Rev. B* **33**, 1026 (1986).
- ¹¹A.-B. Chen and A. Sher, *Phys. Rev. B* **23**, 5360 (1981).
- ¹²M.A. Berding, S. Krishnamurthy, A. Sher, and A.-B. Chen, *J. Vac. Sci. Technol. A* **5**, 3014 (1987).
- ¹³A.-B. Chen and A. Sher, *Phys. Rev. B* **5**, 2897 (1972).
- ¹⁴J.C. Brice, *Properties of HgCdTe*, EMIS Data Review Series No. 3, p. 103 (1986).
- ¹⁵S.M. Sze, *Physics of Semiconductor Devices* (Wiley, New York), p. 22 (1981).
- ¹⁶J. Bajjj, private communication (1993).
- ¹⁷J. Bajjj, S.H. Shin, G. Bostrup, and D.T. Cheung, *J. Vac. Sci. Technol.* **21**, 244 (1982).

**18S. Krishnamurthy and A. Sher, Proc. of IRIS Materials Specialty Group Meeting, Boston,
16 August (1993).**

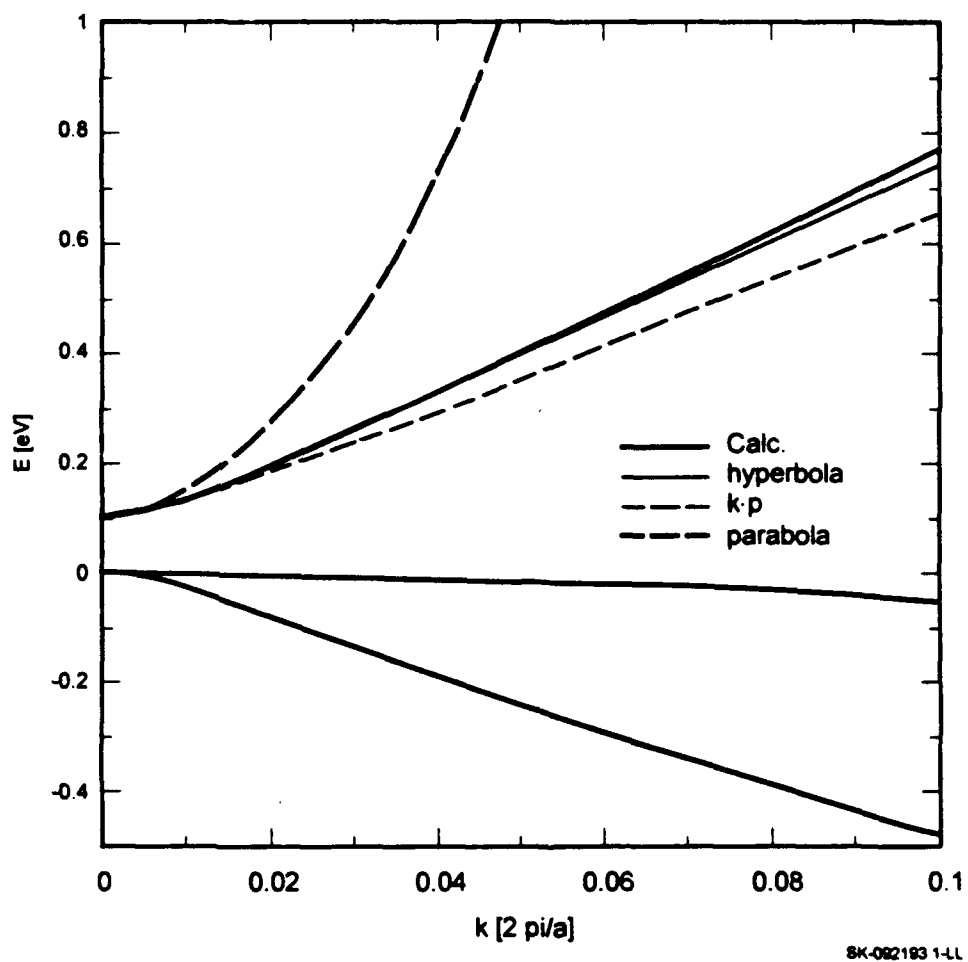


FIG. 1. Electronic structure of $\text{Hg}_{0.78}\text{Cd}_{0.22}\text{Te}$

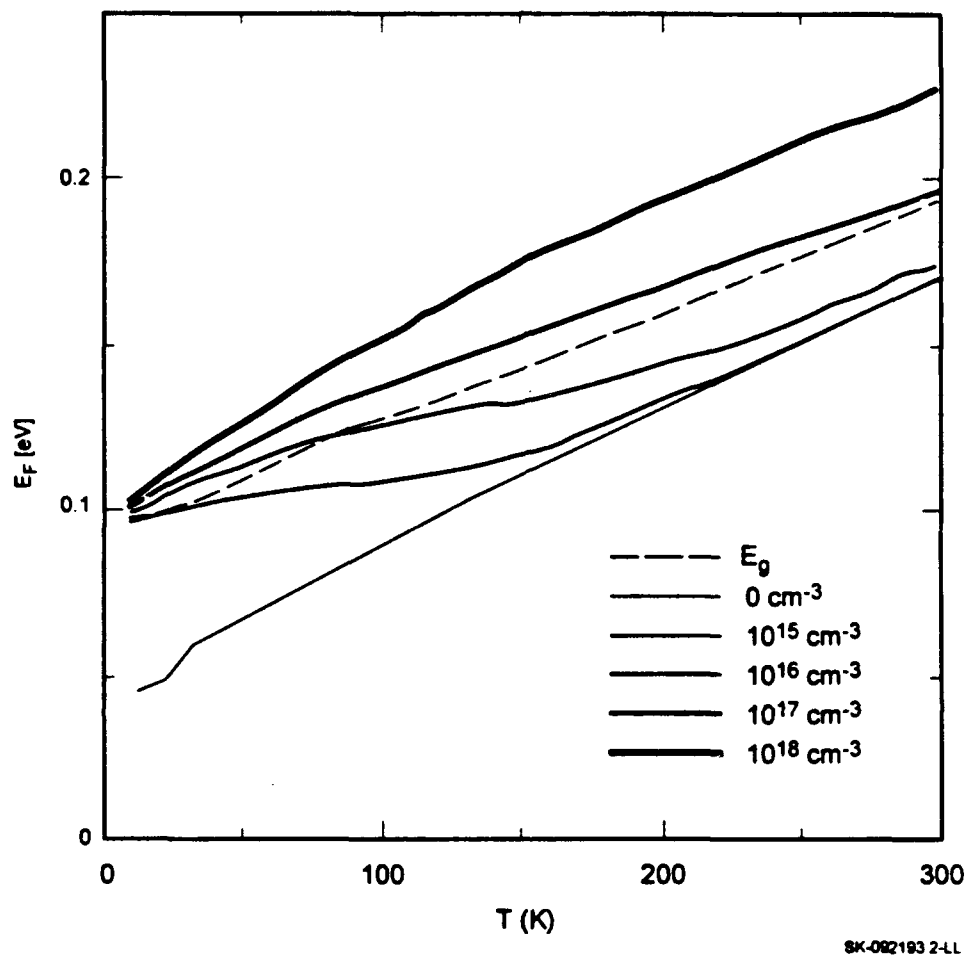


FIG. 2. Fermi energy as a function of temperature: hyperbolic bands

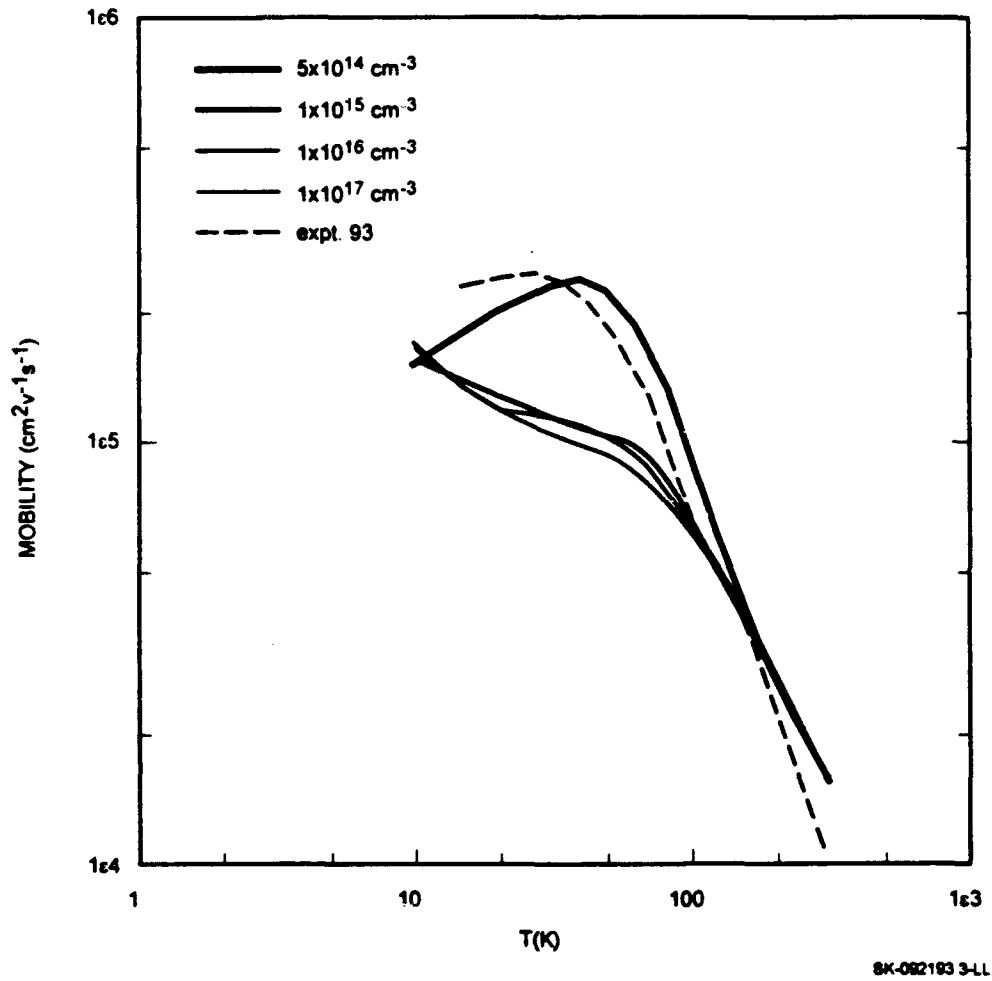


FIG. 3. Drift mobility as a function of T for various impurity combinations

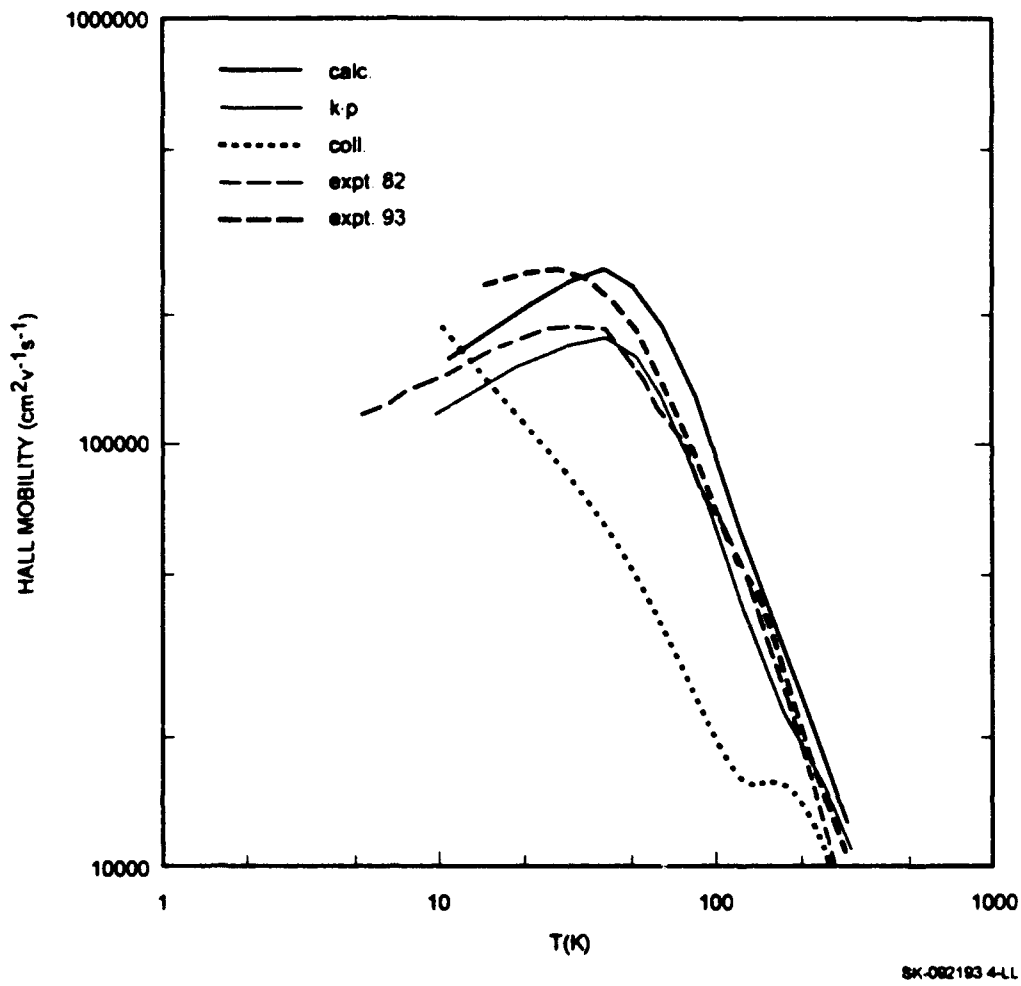


FIG. 4. Hall mobility as a function of T with various approximations